**Rare Metal Materials and Engineering**
Volume 54, Issue 2, February 2025
Available online at www.rmme.ac.cn

Science Press

**Cite this article as**: Sainath Krishna Mani Iyer, Karuppasamy Ramasamy, Prabagaran Subramaniam. Formulation and Characterization of Functionally Graded Materials Comprising SS316L and Inconel625 for Enhanced Performance in High-Pressure Pneumatic Tools[J]. Rare Metal Materials and Engineering, 2025, 54(02): 363-376. https://doi.org/10.12442/j.issn.1002-185X.20240782.

ARTICLE

# Formulation and Characterization of Functionally Graded Materials Comprising SS316L and Inconel625 for Enhanced Performance in High-Pressure Pneumatic Tools

**Sainath Krishna Mani Iyer[1], Karuppasamy Ramasamy[1], Prabagaran Subramaniam[2]**

*[1] Department of Mechanical Engineering, Faculty of Engineering, Karpagam Academy of Higher Education, Coimbatore 641 021, India; [2] Karpagam Innovation and Incubation Council, Coimbatore 641 021, India*

**Abstract:** SS316L alloy coupled with Inconel625 alloy were combined with Ti6Al4V or Inconel718 alloy through wire arc additive manufacturing technique to manufacture functionally graded materials (FGMs). Two FGMs, namely 60% SS316L+20% Inconel625+20% Ti6Al4V composite and 60% SS316L+20% Inconel625+20% Inconel718 composite, were prepared. The tensile strength, elongation, yield strength, hardness, cross section area of the parent material, and composition were analysed. Results illustrate that the 60% SS316L+20% Inconel625+20% Inconel718 composite has better mechanical properties than 60% SS316L+20% Inconel625+20% Ti6Al4V composite, and the comprehensive properties of 60% SS316L+20% Inconel 625+20% Ti6Al4V composite are better than those of the parent material SS316L. Hence, the composite of 60% SS316L+20% Inconel625+20% Inconel718 is optimal. Due to its high strength, the 60% SS316L+20% Inconel625+20% Inconel718 composite has great application potential in the field of high pressure pneumatic tool and defence tool.

**Key words:** microstructure; tensile strength; functionally graded material; additive manufacturing; Inconel alloy; titanium; stainless steel; wire arc additive manufacturing

Functionally graded material (FGM) is a merged compound with advanced structure and innovative function, which has good overall performance and thus can satisfy different requirements even in the harsh environment. Laser direct metal deposition (LDMD) is an innovative manufacture method with mass reduction and energy saving characteristics to manufacture objects of complex geometries[1].

Additive manufacturing (AM) procedure uses CAM/CAD models to prepare three-dimensional (3D) products. Based on ISO/ASTM 52900-15 standard, AM procedures include material extrusion, directed energy deposition (DED), Vat photopolymerization, powder bed fusion (PBF), binder jetting, and sheet lamination (SL)[2]. Until today, AM can be used to prepare various materials[3]. Metal additive manufacturing (MAM) procedure uses arc, laser, and electron beam as the main sources of heat. AM processes for metal materials predominantly include PBF[4], SL, and DED. To be more specific, PBF with laser beam as heat source (PBF-L)[5], DED through gas metal arc (DED-GMA), and DED with laser beam as heat source (DED-L) [6]. Based on the solid raw materials, commonly used AM processes for metal materials can be categorised into wire-based and powder-based systems.

DED technique is normally used for the construction of net-shaped components. In DED process, to-be-deposited material is usually delivered via blown powder or wire feeding. The feeding procedure involves the laser-caused melt pool at the dynamic equilibrium. The deposited metal is heated through laser to the temperature over melting point (usually 3000 °C), followed by prompt solidification[7]. Moreover, WAAM machines can be effortlessly amended from arc welding robots, which are usually less expensive than PBF-L machines. In WAAM procedure, the wire is heated to liquid state and then transported to the melt pool, so the deposited material is firstly hardened at the border of melt pool[2]. The

Received date: December 03, 2024
Corresponding author: Sainath Krishna Mani Iyer, Master of Engineering (M. E.), Department of Mechanical Engineering, Faculty of Engineering, Karpagam Academy of Higher Education, Coimbatore 641 021, India, E-mail: sainath0318@gmail.com

mechanical properties of WAAM-fabricated substances are comparative to those of wrought or cast materials. Viable WAAM processes are in urgent need. Currently, WAAM application is restricted by the heat input, which instigates numerous supplies processing defects and challenges[8].

In spite of straight transition zone (caused by lack of progressively mixed metal fillers) usually occurring in stainless steel (SS) base metal, WAAM works at SS316L and Inconel625 FGMs, which is occasional as well as contradictory. Therefore, the latest work to enhance and associate the properties of FGM is constructed through variant accumulation schemes. Besides the fact that it would be presented via WAAM, an entirely even conversion could be attained, deprived of any defects, which is nevertheless attained additionally based upon AM procedure of fusion[9]. WAAM-shaped welding was utilized to produce the most significant nuclear components in the period of the 20th century via German. Until today, WAAM is utilized in nuclear energy, architecture (bridge steel), aerospace (ribs, panels which are stiffened, wing), and marine (propeller of the ship) industries. Few commercial machines of WAAM have been technologically advanced, and technologies of WAAM have appealed the consideration of diverse research institutions all over the world[9].

FGM can be categorised into different variations in the terms of structure[10] and size. Based on the thickness, FGMs can be categorised into bulk and thin FGMs, and they are also classified as intermittent and unremitting FGMs based on the type of grading[11]. One more type of FGM is graded in structure of porosity or lattice. This kind of FGM might have one single material. The grading is signified by progressively dispersed structure in porosity or lattice instead of chemical composition[12]. Conservative manufacturing procedures for FGMs predominantly consist of powder metallurgy[13], vapour deposition (VD), and centrifugal casting methods[14]. VD is mainly utilized in the fabrication of thin FGM. It is not really an economical way to fabricate the bulk FGMs because of consumption of extraordinary energy with the unhurried process[15]. In order to manufacture bulk FGMs, centrifugal casting and powder metallurgy are superior choices[16]. Using the powder metallurgy to fabricate FGMs includes preparation of stacking, powder mixture, and sintering[14]. As the mixing of powder has been done earlier than the sintering, stepwise grading can only be realised by powder metallurgy. Centrifugal casting can produce unremitting grading through the aid of centrifugal force[14]. The centrifugal casting is restricted because it can merely fabricate cylindrical parts[17]. The entire conservative procedures are time-intensive because several tools and processes are needed. Currently, AM is constructed for bulk FGM parts[18].

Based on the statement of functionally graded plates which behaves like homogenous plates, correlation of the natural frequencies of isotropic and FGM plates can be obtained. An isotropic material equivalent to FGM can be calculated through density and elasticity modulus. The frequency parameters can be evaluated through Eq.(1–3)[19], as follows:

$$E_{eq}=E_tV_t+E_bV_b \quad (1)$$

$$\rho_{eq}=\rho_tV_t+\rho_bV_b \quad (2)$$

$$\Omega_{eq}=\sqrt{(\rho_{ts}E_{eq})/(\rho_{ts}E_{eq})}\Omega_{ts} \quad (3)$$

where $E$ is the Young's modulus; $V$ is the volume fraction; $\rho$ is the mass density; subscript t, b, and eq represent top, bottom, and equivalence, respectively; $\Omega$ is frequency.

The construction in amalgamation of titanium alloys and SS is of main interest in the aerospace[20] and nuclear[21] industries in the terms of corrosion resistance and strength of both the alloys, as well as the low density of titanium. Anyhow, conjoining SS along with titanium and its alloys by joining in liquid phase as well as friction stir welding is difficult, because of the formation of intermetallic phases in the liquid phase combining period of these binary alloy systems[22]. These intermetallic phases (B2 and Laves C14 phases) regularly result in cracking and delamination during the fabrication process[23]. Even the specimens which have no superior defects in the constructed situation may have cracks that form during the post processing of heat treatments, leading to the growth of detrimental phases or the extra thermal stresses[24–25].

Sahasrbudhe et al[26] inspected directly combined Ti6Al4V and SS316L prepared by DED. X-ray diffraction (XRD) analysis exposed the occurrence of $Cr_2Ti$ (Laves), $Fe_2Ti$, and FeTi (B2) phases which are intermetallic compounds at the Ti6Al4V/SS316 interface, which results in the microcracks. In order to diminish the consequences of direct combination of Ti alloys or Ti with SS, intermediate elements are studied as potential buffer deposits to stop the direct mixing of liquid in Fe as well as Ti, which results in the formation of intermetallic phases, such as NiCr, V, Ni, and Cu[27]. Li et al[28] studied Ti6Al4V as well as SS316L by depositing untainted layers of V, Fe, and Cr onto a baseplate of SS316L. Sahasrabudhe et al[26] fabricated a model which is utilized in a bond layer of NiCr between the SS316 and Ti6Al4V layers. XRD analysis revealed evidence of $Cr_2Ti$ existence at the Ti6Al4V/NiCr interface. Meanwhile, neither microcracks nor defects were found in this model. $Cr_2Ti$ is a phase of brittle intermetallic compound, which could result in cracking[25].

According to Ref. [1], research about FGM prepared by LDMD predominantly concentrates on the process of forming and the analytic properties. Balla et al[29] found that the deposition of $TiO_2$ particles on the porous Ti matrix mainly optimized the hardness and wettability of the matrix. Besides, the non-hazardous and graded structure which is biocompatible along with concentration of vibrational $TiO_2$ could develop the capability to form lubricated chemical film and decrease the friction coefficient of polyethylene, which decreased the wear rate of material. Carroll et al[24] fabricated 304L/Inconel625 FGM by LDMD which has obvious and structural limit, and the phase stability of the material was calculated by thermodynamics simulation[1]. Meanwhile, in the current study, three FGMs were fabricated for analyzing the mechanical properties of parent material. The study intended to optimize the parent material SS316L and to enhance its mechanical properties

through the addition of three FGMs, such as Inconel625, Inconel718, and titanium. The study formulated the parameters of FGM composition using Eq.(1–2).

Fig. 1 illustrates the working module of WAAM and exact images of welding machines. Fig. 1a shows the welding table used in the current study. Fig. 1b shows the robotic welding arc which has been employed in the study. Fig. 1c shows the welded SS and Fig. 1d shows the robotic controller of WAAM. Fig. 2 illustrates the systematic process of WAAM. The material characteristics are optimized by means of WAAM and also several key parameters are determined for the optimization. The parameters are travel speed, deposition strategy or path planning, wire feed rate, arc voltage, and working distance. The wire is melted though the process of heating with support of electric arc. Later, it is transferred to the molten pool. Finally, through the solidification process, a layer-by-layer material is formed.

## 1 Research Scheme

### 1.1 Problem definition

SS contains chromium. Once it is unprotected in oxygen atmosphere, a thin imperceptible layer considered as chromium oxide is formed. Rust will be generated once this deposit is impaired when the material is in contact with chloride, which is usually contained in the environment of high salinity, cleaners, high humidity, and mechanical abrasions[30]. To acquire high quality parts of WAAM-prepared SS, at present, the strong need is essential for upcoming research about the primary mechanisms in the physical metallurgy procedure in WAAM, the upcoming heat treatments to enhance WAAM, and the parametric heat treatment which controls the microstructure[2]. Cost is higher for SS316. The raised contents of molybdenum and nickel contribute to the high price. Engineers should carefully evaluate the benefits in relation to the costs to assess its suitability for a particular application. When it comes to machinability, SS316 is considered more challenging to machine compared to other grades of austenitic SS. Its rigidity, along with its tendency to work hardening, can lead to decreased tool life and increased machining time, which negatively impacts production efficiency. Regarding welding challenges, although common procedures can successfully weld SS316, the risk of sensitization, resulting from the formation of chromium carbides at the grain boundaries, can lead to reduced corrosion resistance in the heat-affected zones. Proper welding techniques and post-weld treatments are essential to mitigate these issues. Due to its propensity to adhere to mating surfaces under pressure, SS316 is susceptible to galling and scoring, particularly in applications involving friction or sliding. Careful selection of surface finishes and lubricants can help alleviate these concerns. In terms of design complexity, the optimized corrosion resistance and mechanical properties of SS316 often require specific design considerations, including material thickness, joint configurations, and fabrication methods. Failing to account for these factors could result in suboptimal performance or production difficulties[30].


Fig.1 Appearances of welding table (a), FANUC Arc Mate 100iC Robotic machine (b), welded SS (c), and robot controller (d)

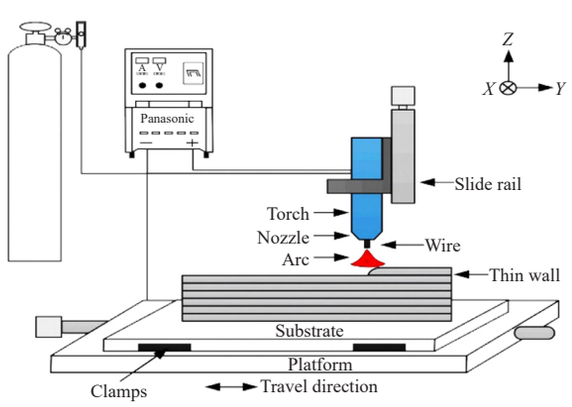


Fig.2 Schematic illustration of WAAM

### 1.2 Research objects

In this research, the research objects are as follows: (1) manufacture SS316L as main material using WAAM; (2) manufacture FGM of SS316L+Inconel625+Ti6Al4V (titanium grade 5) using WAAM; (3) manufacture FGM of SS316L+Inconel625+Inconel718 using WAAM; (4) analyse the mechanical properties of SS316L and compare them with those of FGM (SS316+Inconel+titanium); (5) manufacture FGM using WAAM.

FANUC ARC Mate 100iC Welding Robot is a 6-axis robot designed for intermittent programming tasks such as welding and cutting. It can handle mass of up to 12 kg. The robot can efficiently manage all essential cables and wires through its body. It is equipped with a Fronius TPS 400i power source welder and an R-30iB controller. In terms of specifications, the FANUC ARC Mate 100iC is engineered for reliability and exceptional performance in welding applications. The airline cable for the welding torch, along with gas lines and other cables, are routed through the robotic manipulator for safety. This design reduces setup time and ensures that the cables do

not interfere with one another. The 100iC robot can consistently operate at high speeds while supporting loads of up to 12 kg. It features a compact wrist that allows it to manoeuvre in tight spaces within the workspace. This robot utilizes two types of coordinate systems: joint coordinates and Cartesian coordinates. The robot's position is defined using angular positions in the joint coordinate system, allowing individual joints to be moved independently. The Cartesian coordinate system and joints can be relocated individually. The Cartesian coordinate structure's coordinates moreover supplies position, ability, and orientation of tool to relocate the robot linearly or adjust its orientation. The robot can reach distance of 1098 mm, allowing it to operate in various positions, including different angles even inverted relative to the floor. To ensure safe operation, recommended safety protocols must be detected[31].

### 1.3 Significance of study

The present study analyses the parent material and the construct novel materials by the addition of FGM. FGMs with three components have been proposed in the current study. Most of the previous studies have focused only on the FGM of two phase components. Also, most of the studies have utilized powder metallurgy technique for manufacturing the FGM. Nonetheless, WAAM is considered to be the most significant technique for the manufacturing of FGM. Hence, the present study employs WAAM technique for generation of three FGMs. This novel approach is significant for the defence application. The study has chosen SS316L as the parent material which has been combined with Inconel and titanium alloys. The newly identified combinations are subjected to various tests in order to predict the high pressure pneumatic ability. The designed FGMs are SS316L, 60% SS316L+20% Inconel625+20% Ti6Al4V, and 60% SS316L+20% Inconel625+20% Inconel718. The new combination of FGM contributes to the high pressure pneumatic application.

## 2 Literature Review

In this research, FGM[1] along with the composition variable from 100% SS316L towards 100% Inconel625 alloy was fabricated effectively utilizing LDMD technique. Mechanical properties, composition, grain morphology, and abrasive resistance were attained to inspect the microstructure and the FGM mechanical properties. Through the growth in content of Inconel625, spacing of major dendrite arm has increased. In addition, the second white phases start to precipitate alongside boundary of dendrites once the Inconel625 content exceeds 80%.

Microhardness progressively improved from 2121.504 MPa of the lowest graded FGM to 3485.860 MPa of the highest graded FGM. This increase in microhardness, along with the rise in the volume of hard phases, has led to a reduction in the wear rate of FGM and an optimization of its wear resistance. Analysis of the fracture elements revealed a significant number of small unevenly dispersed second phases, which contribute to fractures in FGM. Additionally, the tensile fracture mechanism involves the typical accumulation of micropores, which affects toughness. In the current study, LDMD was employed to fabricate Inconel625/SS316L without cracks, ensuring appropriate distribution of hard phases and a strong metallurgical bond between the deposited layers of FGM. The microstructure of materials was examined to assess grain morphology, and the effects of deposition process on microhardness, wear resistance, fracture properties, and tensile properties of FGM were further analysed to evaluate its performance.

In Ref.[32], FGMs of SS316L and nickel-based superalloy (Inconel625) were produced using gas metal arc welding (GMAW) -ground WAAM. The microstructural analysis revealed a significant evolution in the interfacial region, characterized by a suspended decorative structure. Energy dispersive spectroscopy (EDS) investigations confirmed sufficient dissolution of elements at the interfacial region with no significant variations detected in the composition. Electron backscattered diffraction (EBSD) was conducted for analysis. EBSD results indicated that the particles were predominantly columnar, while the interfacial region exhibited uniform crystallographic development along with large elongated dendrites oriented in the <001> direction. The microstructure of the SS316L layers was primarily austenitic with a smaller proportion of ferrite. Precipitates were observed within the layers of Inconel625, embedded in the austenitic matrix. The ultimate tensile strength (UTS) and yield strength (YS) of Inconel625 and SS316L were comparable to those of processed materials. The entire interfacial region specimens, oriented at 90°, exhibited lower UTS in the SS316L region compared to Inconel625, and the fracture mode was ductile. Microhardness measurements demonstrated a gradual transition in hardness along the building direction. This study highlights the potential of WAAM for fabricating FGMs with essential properties, presenting a viable alternative to conventional manufacturing techniques for producing FGMs.

In Ref. [2], the current status of WAAM-prepared SS is explained, covering defects, microstructure, and mechanical properties related to distinct parametric processes and SS. The discussion includes WAAM-manufactured components, such as distortion and residual stress. Key factors in WAAM that significantly impact the mechanical properties of SS include the specific techniques, material composition, defects, process parameters, microstructure, shielding gas composition, and post-heat treatment. To achieve exceptional quality in WAAM-prepared SS parts, there is a pressing need for further research into the underlying mechanisms of physical metallurgy to enhance WAAM and the parametric heat treatment that governs microstructure. WAAM specimens often exhibit anisotropy, which is significant in both mechanical properties and microstructure. WAAM has been demonstrated to be an affordable and highly effective AM process, especially when compared to PBF, for producing complex parts of SS. Recent research on various WAAM-prepared SS has been conducted from the perspective of macroscopic features, microstructure evolution, post-heat treatment, defects, distortion, residual

stress, and mechanical properties.

In Ref. [9], a FGM composed of SS316L and Inconel625 was constructed using various deposition strategies, referred to as smooth type and direct interfaces, through arc AM and twin-WAAM techniques. This combination of materials is primarily utilized in the oil, gas, and nuclear industries, as well as in chemical plants, where extreme corrosion resistance and wear resistance are essential requirements. Although Inconel625 exhibits superior properties, replacing Inconel625 with SS316L in specific structural components can reduce overall costs and decrease the mass of the parts. Both the smooth and direct conversion interfaces were verified and characterized. Microscopic analysis demonstrated that each interface, along with the constructed specimen, possessed an austenitic matrix, and all specimens were well-bonded and free of defects. Various microstructures developed at the interfaces due to the differing gradients in composition. Measurements obtained from synchrotron X-ray diffraction (SXD) indicated the presence of evenly distributed secondary phases, such as the d phase ($Ni_3Nb$) and carbides, which were absent in the alloys prepared by direct interface strategy. The proportions of fracture locations in the smooth and direct transition interfaces were found as 65% and 50% of those in SS region, respectively. The specimens exhibited significant ductile fractures with considerable plastic deformations during the tensile tests. Measurements of residual stresses, obtained through neutron diffraction, revealed stresses at FGM interfaces.

In Ref. [33], dual-wire arc manufacturing was employed to fabricate FGM with a uniform alignment transition from 100% Inconel625 to 100% SS308L, featuring consistent compositional changes in the direction of torch travel. By varying the composition, the fragile melting temperature can be clearly and easily positioned along the composition gradient, allowing the issue to be fully addressed. During the fabrication process, cracks were observed near the region containing 20% Inconel625. Analysis of the morphology and location of the cracks indicated that they were liquation cracks, which are a type of hot crack. Based on the experimental results and phase diagram calculations, it was determined that cracks consistently formed near the area with 20% Inconel625, where FGM exhibited maximum sensitivity to cracking. This finding identifies the fragile region of FGM and simplifies the understanding of its weakening mechanism, particularly in relation to the compositional transition. This insight provides a greater opportunity to enhance mechanical properties through targeted optimization. Parametric process optimization decreases the input of heat with unit height to dendrites which are thin, and it also improves the cracking. However, it seems to be a tendency of cracking in the composition range which is weak. Through the elimination of consistent range in composition, the gradient path of the optimization in composition can solve the issue in cracking much thoroughly. Besides, tensile strength and elongation are raised by 39.5% and 221.7%, respectively, indicating huge enhancement in the mechanical properties of FGM.

In Ref. [34], the determination of FGM was conducted through AM using DED and laser synchronous preheating (LSP). The material includes Inconel625 and Ti6Al4V. The research focuses on the development of microstructure, crack behavior, phase characteristics, and microhardness as functions of the composition within the graded material. Cracking primarily occurred in the transition zone. A sequence of phase developments was observed with the increase in proportion of Ti6Al4V. The maximum hardness was achieved when the material composition was 60% Inconel625 and 40% Ti6Al4V, which is significantly influenced by the presence of multiple phases. LSP played a crucial role in enhancing deposition and suppressing cracking during the laser deposition of Inconel625/Ti6Al4V-graded material. This research demonstrates that LSP is the most effective method for improving crack suppression and deposition quality in the laser fabrication of FGMs composed of Inconel625 and Ti6Al4V.

Ref. [2] focused solely on the microstructure of the specimen, mechanical properties, process parameters, post-heat treatments, and material composition, as well as WAAM technique. For future industrial applications, the fatigue properties and corrosion behavior of WAAM-prepared SS need to be thoroughly investigated in the coming years. Additionally, further efforts must be made to enhance WAAM process to achieve higher deposition rates and improved quality control.

Ref. [33] focused solely on the cracks that occur during tests of elongation and microhardness. However, it did not address the SEM analysis, X-ray diffraction (XRD) analysis, or the microstructure of FGM.

Ref. [34] focused solely on the two-phase FGM with the parent material. Therefore, a forward-looking approach is necessary for the three-phase FGM along with the analysis of all critical parameters.

## 3 Experiment

### 3.1 Specimen preparation

FGMs were prepared using SS316L, Inconel625, and Ti6Al4V. The details of welding wires made of titanium, with diameter of 1 mm, are shown in Table 1. A gas tungsten arc welding (GTAW) system, specifically the great tool spitfire TIG DC 1700 power source, was employed. This power source requires a high-frequency start, which enables the electric arc to initiate without direct contact between the non-consumable tungsten electrode and the substrate. An internal multiple-wire feed system was utilized for the tests conducted in Ref. [35]. Fig. 3 illustrates the SS316L FGM specimen from the current study.

Table 1 shows the chemical composition of Ti6Al4V, Inconel625, SS316L, and Inconel718 alloys. The key features and related applications of the experiment materials are listed in Table 2.

### 3.2 Fabrication

Powder particles were re-joined and compressed to form

**Table 1 Chemical composition of Ti6Al4V, Inconel625, SS316L, and Inconel718 alloys (wt%)**

| Ti6Al4V | | Inconel625 | | SS316L | | Inconel718 | |
|---|---|---|---|---|---|---|---|
| Element | Content | Element | Content | Element | Content | Element | Content |
| Fe | 0.22 | C | 0.10 | C | ≤0.03 | C | 0.08 |
| O | 0.12–0.20 | Mn | 0.50 | Mn | ≤2.00 | Mn | 0.35 |
| C | 0.05 | Si | 0.50 | P | ≤0.045 | Ti | <1.00 |
| N | 0.03 | P | 0.015 | S | ≤0.030 | Co | <1.00 |
| H | 0.015 | S | 0.015 | Si | ≤0.75 | Si | 0.35 |
| Al | 5.50–6.75 | Cr | 23.00 | Cr | 16.00–18.00 | Cu | 0.30 |
| V | 3.50–4.50 | Co | 1.00 | Ni | 10.00–14.00 | Nb | 5.00 |
| Ti | Bal. | Mo | 10.00 | Mo | 2.00–3.00 | Mo | 3.00 |
| - | - | Fe | 5.00 | N | ≤0.10 | Al | 0.80 |
| - | - | Al | 0.40 | - | - | - | - |
| - | - | Ti | 0.40 | - | - | - | - |
| - | - | Ni | - | - | - | - | - |
| - | - | Nb/Cb | 4.15 | - | - | - | - |
| - | - | Ta | 0.05 | - | - | - | - |
| - | - | Cu | 0.50 | - | - | - | - |

Fig.3 Appearance of SS316L FGM

the required shape. The heating of the material was also conducted[36].

Utilizing powder metallurgy to fabricate FGMs involves several key processes, including stacking, powder mixing, and sintering. The mixing of powders and stacking must be completed prior to the final sintering, as the metallurgy of the powder can only be achieved through stepwise grading. The method of centrifugal casting enables continuous grading through the application of centrifugal force. However, the restriction of centrifugal casting is that it can only produce cylindrical parts. Traditional methods tend to be time-consuming, as they require numerous tools and assembly processes. Nevertheless, WAAM is a significant method for producing FGM. Therefore, this study employs the WAAM method to manufacture a three-phase FGM to optimize the parent material.

The fabricated components consist of distinct walls, measuring 130 mm in length, with a current of 65 A applied to each material. A mild steel plate (180 mm×50 mm×6 mm) was used as the substrate. The selection of preliminary parameters facilitated an appropriate parametric process, resulting in identical width and height for materials. These parameters are instrumental in fabricating the specimens listed below: (1) five specimens of 100% 316L stainless steel; (2) five specimens of FGM composed of 60% SS316L, 20% Inconel625, and 20% Ti6Al4V; (3) five specimens of FGM composed of 60% SS316L, 20% Inconel625, and 20% Inconel718[9], as shown in Fig. 4. The material details and process parameters are listed in Table 3 – 5. Metal-inert gas welding was also employed.

### 3.3 Testing methods

Specimens were polished, cut, and then fixed individually. Before conducting microscopic observations, the specimens were refined using abrasive paper with grits ranging from 80# to 2000#. Additionally, they were polished with diamond suspension of 1 mm. The entire specimens were imprinted electrolytically using a 10wt% chromium trioxide ($Cr_2O_3$) solution, which was dissolved in distilled water and applied at a potential of 5V for 20 s. Microstructural examinations were performed using a Hitachi SU3800 scanning electron microscope (SEM) and a Zeiss 1530 field emission SEM, both well-prepared with EDS.

**Table 2 Key features and applications of experiment materials**

| Key feature | Application |
|---|---|
| Outstanding corrosion resistance in an extensive region of corrosive media | Marine industries<br>Aerospace industries<br>Chemical processing |
| Superior resistance against pitting and crevice corrosion | Nuclear reactor |
| Better for sea water applications | Pollution control |

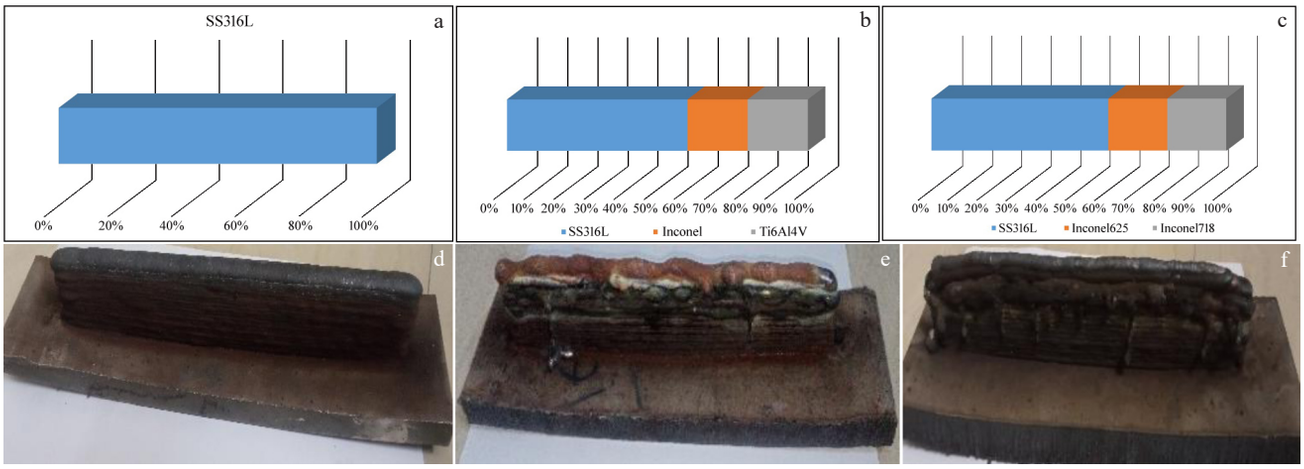


Fig.4 Schematic diagrams (a–c) and appearances (d–f) of SS316L (a, d), 60% SS316L+20% Inconel625+20% Ti6Al4V (b, e), and 60% SS316L+20% Inconel625+20% Inconel718 (c, f)

**Table 3 Typical chemical composition of undiluted weld metal (wt%)**

| C | Mn | Si | Cr | Ni | Mo |
|---|---|---|---|---|---|
| 0.03 | 1.7 | 0.4 | 18.3 | 11.5 | 2.2 |

**Table 4 GTAW process parameters for SS316L/Inconel625 FGM fabrication**

| Parameter | Value |
|---|---|
| Travel speed/mm·min$^{-1}$ | 120 |
| Wire feed speed/m·min$^{-1}$ | 1 |
| Average current/A | 65 |
| Shielding gas | Argon (99.9%) |
| Shielding gas flow rate/L·min$^{-1}$ | 16 |

The microhardness testing was conducted using a Mitutoyo HM112 hardness testing machine. Measurements were taken in a straight line, starting from the substrate and progressing towards the final accumulated layer of each specimen. The distance between indentations was set at up to 250 mm with the applied load of 4.9 N. A four-point potential drop technique, as previously defined in Ref.[37], was employed to detect changes in electrical conductivity among the specimens. Measurements were taken across the entire height with a spacing of 635 mm and an applied current of 80 mA. Uniaxial tensile tests were performed on an MTS servo-hydraulic press with a capacity of 100 kN and a displacement rate of 1 mm/min. Specimens were arranged so that the transition between materials was precisely at the center of the tensile specimens. Digital image correlation (DIC) during tensile testing was conducted using the 2D DIC MATLAB software toolbox. The anisotropy of tensile strength significantly affects the performance of AM-prepared components. Consequently, post-heat treatments, WAAM techniques, shielding gas composition, material composition, processing parameters, as well as defects and microstructure can predominantly influence the mechanical properties of SS produced by WAAM[2]. Table 6 shows the process parameters affecting morphology of WAAM-prepared SS parts.

## 4 Results and Discussion

### 4.1 Microstructure analysis

The microstructures of SS prepared by WAAM are significantly influenced by the thermal history during the processing. During WAAM, the thermal cycle, which includes continuous heating and cooling, generates equilibrium microstructures in the deposited layers. Table 7 presents YS, elongation, and tensile strength of SS produced by various WAAM technologies. The factors affecting mechanical properties and microstructure are also listed in Table 7. Due to the varying heating conditions and thermal cycles across different regions of the deposited specimens, the microstructures are categorized into three distinct areas: upper, center, and lower. The mechanical properties, macrostructure, and microstructures of the center section are particularly critical for the performance of the manufactured components.

**Table 5 Actual process parameters of MIG+WAAM for fabrication of SS316L, Inconel625, Ti6Al4V, and Inconel718**

| Parameter | SS316L | Inconel625 | Ti6Al4V | Inconel718 |
|---|---|---|---|---|
| Travel speed/mm·s$^{-1}$ | 4 | 4 | 5 | 4 |
| Average current/A | 180 | 160 | 140 | 155 |
| Shielding gas | 80% argon and 20% $CO_2$ | 85% argon and 15% $CO_2$ | 95% argon and 5% $CO_2$ | 85% argon and 15% $CO_2$ |
| Cooling time between layers/s | 90 | 120 | 140 | 130 |

**Table 6 Process parameters affecting morphology of WAAM-prepared SS parts**

| WAAM Technique | Material | Process parameter | Macroscopic characteristic | Ref. |
|---|---|---|---|---|
| MIG | 316L (austenitic) | Mode of welding current; gradual decrease of bottom current | More bottom formation | [38] |
| | | Increasing scanning speed | Unevenness of both ends | |
| Plasma additive manufacturing (PAM) | H00Cr21Ni10 (austenitic) | Single-wire feed (SWF) and PAM | Slightly better surface quality than that prepared by double-wire feed (DWF) and PAM | [39] |
| SWF-PAM, DWF-PAM | | DWF-PAM | - | |
| | | Increasing scanning speed | Better surface quality | |
| GMAW | Type-2209 (duplex) | Deposition path: Alternating direction deposition path | Uniform layer height | [40] |
| | | Deposition path: One-direction deposition path | Uneven sides: the start side was higher than the end side | |
| GMAW | H08Mn2Si low-carbon steel | Decreasing interlay temperature | Decreased surface roughness | [41] |
| | | Increasing scanning speed | Decreased surface roughness | |
| | | Increasing wire feeding speed | Decreased surface roughness | |

**Table 7 Average values of mechanical properties**

| Parameter | SS316L | 60% SS316L+20% Inconel625+20% Ti6Al4V | 60% SS316L+20% Inconel625+20% Inconel718 |
|---|---|---|---|
| UTS/MPa | 506 | 686 | 1096 |
| YS (0.2% proof)/MPa | 266 | 339 | 672 |
| Elongation/% | 46 | 44 | 39 |
| Hardness/HRC | 12 | 16 | 20 |
| Cross sectional area/% | 86.1 | 75.5 | 36.7 |
| Hardness, HB/MPa | 1822.8 | 1989.4 | 2185.4 |

The ferrite phase was deposited on the uniform matrix of austenite with each layer comprising a series of fine-grained, equiaxed, and columnar grain regions, arranged from lower to upper region. The distribution of elements in FGM specimens was analysed using SEM/EDS.

Fig.5 illustrates the microstructures of various experimental materials. The microstructural development in SS316L is influenced by the cooling rates of the product. Microstructural characterization was conducted using SEM. The specimens were prepared until the evaluated surface was free of visible

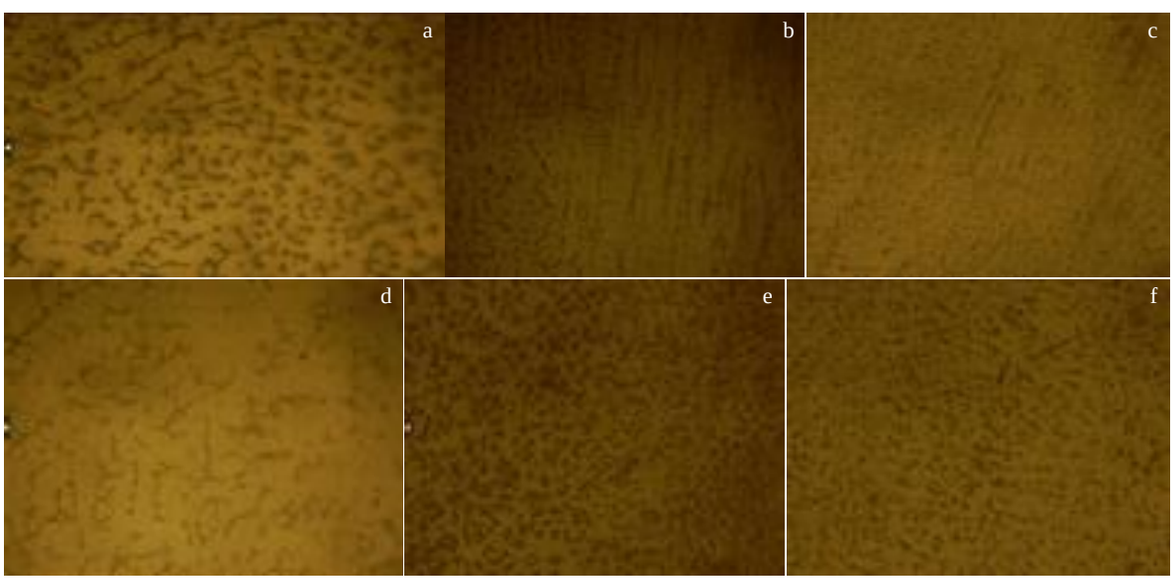


Fig.5 500X microstructures of SS316L (a), Inconel625 (b), Inconel718 (c), Ti6Al4V (d), 60% SS316L+20% Inconel625+20% Ti6Al4V (e), and 60% SS316L+20% Inconel625+20% Inconel718 (f)

scratches. The microstructure is employed to identify defects such as cracks and voids in SS316L, Inconel625, Inconel718, and Ti6Al4V. Additionally, the combinations of 60% SS316L+ 20% Inconel625+20% Ti6Al4V and 60% SS316L+20% Inconel625+20% Inconel718 were evaluated until they formed a uniform structure. Similarly, Feng et al[39] examined the microstructure in the regions adjacent to the processed parts. It is reported that increasing scanning speed results in improved grain structure, specifically finer completely grown equiaxed ferrite (CGEF) grain structures. Furthermore, wires melted in the same melt pool, leading to the formation of a uniform CGEF grain structure. The quantity of CGEF grains primarily develops in the specimens. However, in some specimens, a few incompletely grown equiaxed ferrite (IGEF) grains were observed. As the scanning speed increases, the number of IGEF grains decreases with only a few grains remaining visible. Due to the distribution of CGEF grains in the region of interface adjacent to the subsequent layer, UTS of DWF-PAM-prepared specimens is greater than that of the SWF-PAM-prepared specimens.

Fig.6 illustrates SEM images of FGMs. It can be seen that FGM of 60% SS316L+20% Inconel625+20% Inconel718 shows fine uniformly distributed grains and a well-defined morphology in the microstructure. UTS of DWF-PAM-prepared specimen increases by an average of approximately 10.2%, reaching about 52.98 MPa[39].

### 4.2 Mechanical properties

Existing studies on the mechanical properties of SS structures fabricated through WAAM significantly concentrated on tensile strength and hardness. Although, in several categories, the mechanical properties of WAAM-prepared parts can be compared to those of conventionally machined components, there remains a need to better understand the correlation between the parametric processes and the mechanical properties of WAAM-manufactured parts[42–44]. Research has indicated that heat input during WAAM process has a significant impact on morphology, microstructure, and mechanical properties[45]. Even when the wire feed rate remains constant, the heat input varies depending on the arc mode used[45]. Another factor influencing the mechanical properties of WAAM components is the mode of metal transfer, which affects the rate of liquid droplet transfer, even though the wire feed rate remains unchanged[46–47]. The current study also evaluated the mechanical properties of WAAM. The focus was primarily UTS, YS, hardness, elongation, and cross-sectional area. Table 7 illustrates the average values of the mechanical properties for three FGMs. Among these parameters, UTS and hardness (HB) are presented to facilitate material optimization, as listed in Table 7.

According to WAAM technique, FGM of 60% SS316L+ 20% Inconel625+20% Inconel718 exhibits the highest UTS of 1096 MPa. In contrast, the parent material has the tensile strength of 506 MPa. Although the elongation of the parent material is greater than that of FGMs, other mechanical properties of the FGM are superior to those of the parent material.

#### 4.2.1 Hardness distribution

Vickers hardness of SS316L components exceeds 1715 MPa, which is achieved through both the speed pulse process (the primary mode of metal transfer is a representative form of spray transfer) and the speed arc process (the main mode of metal transfer is the short-circuited conversion mode) in AM process[45].

Although the deposition rates and scanning speeds are similar for both procedures, the speed arc WAAM technique produces an exceptionally solidified structure. The minor spacing of the secondary dendrite arms in the deposited parts results in reduced heat input and a greater cooling rate. Consequently, the hardness values of parts produced by speed arc WAAM are higher than those produced by speed pulse WAAM. It is observed that the hardness value of SS316L specimens gradually decreases from the bottom to the top due to heat accumulation. As illustrated in Table 8, the average hardness in the bottommost phase is somewhat greater than that of the upper region[38]. The hardness results in Table 8 demonstrate that FGM of 60% SS316L+20% Inconel625+ 20% Inconel718 exhibits higher hardness (HB) with an average of 2185.4 MPa.

#### 4.2.2 Tensile strength

WAAM components can be achieved through appropriate parametric processes and a comprehensive understanding of solidification phenomena is discussed[47]. Fig.7–Fig.9 show the tensile test design and results of specimens.

Thompson et al[48] discussed the final aspect of geometry, noting that singularities in localized solidifications significantly affect microstructure, which in turn influences the mechanical properties of the accumulated components[39].

The study investigated the association among microstru-

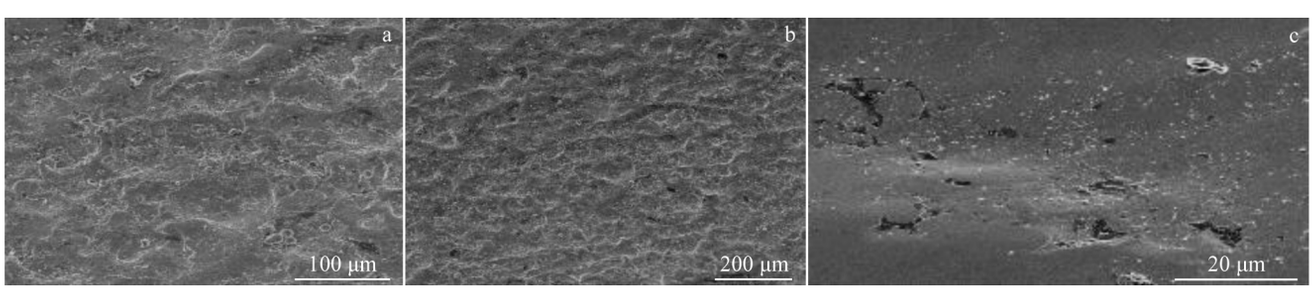


Fig.6 SEM images of SS316L (a), 60% SS316L+20% Inconel625+20% Ti6Al4V (b), and 60% SS316L+20% Inconel625+20% Inconel718 (c)

**Table 8 Hardness results of different experiment materials (MPa)**

| No. | SS316L | 60% SS316L+20% Inconel625+20% Ti6Al4V | 60% SS316L+20% Inconel625+20% Inconel718 |
|---|---|---|---|
| 1 | 1822.8 | 1994.3 | 2185.4 |
| 2 | 1822.8 | 1989.4 | 2180.5 |
| 3 | 1808.1 | 1995.3 | 2185.4 |
| 4 | 1821.8 | 1979.6 | 2184.4 |
| 5 | 1813.0 | 1969.8 | 2185.4 |

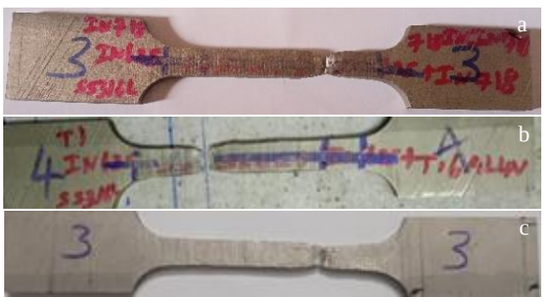


Fig.7 Tensile failure images of SS316L (a), 60% SS316L+20% Inconel625+20% Ti6Al4V (b), and 60% SS316L+20% Inconel625+20% Inconel718 (c)

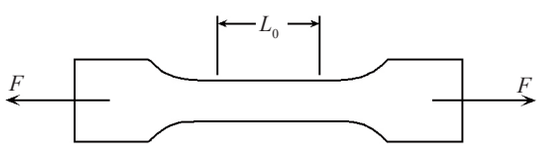


Fig.8 Schematic diagram of tensile test specimen

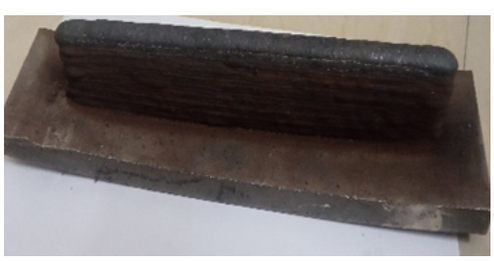

Fig.9 Appearance of flat plate prepared by AM

cture, scanning speed, and UTS. It is identified that the grains of CGEF contribute to the increase in the elongation and UTS of specimens of Cr-Ni SS produced by DWF-PAM or SWF-PAM with scanning speeds ranging from 30 cm/min. UTS and YS are correspondingly dependent on the direction of deposition, which leads to the increased growth of columnar coarse crystals, resulting in anisotropy[2].

Table 9 shows UTS results of three experiment materials. The average UTS of SS316L, 60% SS316L+20% Inconel625+20% Ti6Al4V, and 60% SS316L+20% Inconel625+20% Inconel718 is 507, 686, and 1096 MPa, respectively.

4.2.3 Stress-strain

Fig.10 illustrates the stress-strain curves of different FGMs. It can be seen that 60% SS316L+20% Inconel625+20% Inconel718 has higher UTS. For 60% SS316L+20% Inconel625+20% Inconel718, its UTS is 1096 MPa, YS is 672 MPa, elongation is 39%, hardness is 20 HRC, cross sectional area is 36.7%, and hardness (HB) 2185.4 MPa. For 60% SS316L+20% Inconel625+20% Ti6Al4V, it has properties of UTS of 686 MPa, hardness of 16 HRC, and elongation of 44%.

### 4.3 Tribological properties

Chen et al[1] have identified the mass loss in the tribological curve of specimens. The effects of strengthening with Nb, Ti, and Mo varied gradually alongside Inconel625, leading to an increase in hardness of the materials with enhanced wear resistance[49]. As the content of Inconel625 increases from 60% to 80%, wear resistance improves significantly due to the increased hardness and refined microstructure. Furthermore, there are numerous hard phases that can be utilized to withstand shear forces and support loads, which effectively enhances the wear resistance and reduces the wear rate of materials[1]. One of the most important factors in FGMs prepared through DLD is the appropriate selection of powder mixtures. These mixtures must align with the chemical, metallurgical, and tribological requirements of the components, which is a crucial aspect that promotes improvement[50]. The regulation of particle size and the determination of optimal mixing conditions are essential for producing gradient materials with precise control over microstructure and chemical composition[51]. As the composition of the material varies throughout FGM process, multiple phases with diverse composition are formed. These

**Table 9 UTS of different experiment materials (MPa)**

| No. | SS316L | 60% SS316L+20% Inconel625+20% Ti6Al4V | 60% SS316L+20% Inconel625+20% Inconel718 |
|---|---|---|---|
| 1 | 512.0 | 686.0 | 1096.0 |
| 2 | 506.0 | 686.0 | 1096.0 |
| 3 | 500.0 | 685.9 | 1095.5 |
| 4 | 510.0 | 684.9 | 1095.0 |
| 5 | 506.0 | 685.0 | 1095.9 |

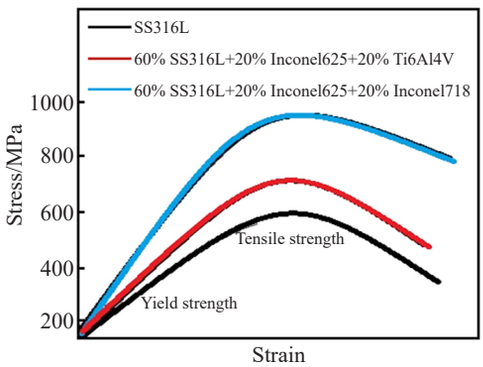


Fig.10 Stress-strain curves of different experiment materials

phases contribute to the desired performance of FGM for the intended application. The formation of these diverse phases primarily depends on the material composition and the manufacturing conditions, including preheating, laser power, feed rate, cooling rate, and scanning speed[52].

The results also indicate that effective fabrication of FGM can be achieved using a direct interface deposition strategy. Specimens prepared for tensile tests were aligned with the load direction corresponding to the build-up direction (*Z*-axis) to evaluate their properties using various deposition techniques.

The reduction in expansion at the fracture can be attributed to the increase in interdendritic phases (both carbides and sigma phase) compared to the control specimen (SS316L) in the area where the fracture occurs (65wt% SS). This mixture results in a detrimental microstructure that causes reduced ductility in relation to FGM. Fractures occur at the center of the specimens (50wt% SS/50wt% Inconel625). A significant gradient between materials results in lower tensile strength and fractures occurring during elongation. The presence of multiple layers with varying ratios makes the material more susceptible to inclusions and precipitates. UTS of 100% SS316L is 506 MPa, whereas that of 60% SS316L+20% Inconel625+20% Ti6Al4V is 556 MPa. In contrast, the 60% SS316L+20% Inconel625+20% Inconel718 exhibits the tensile strength of 1096 MPa. SS316L has YS of 266 MPa, while the 60% SS316L+20% Inconel625+20% Ti6Al4V has yield strength of 339 MPa. The 60% SS316L+20% Inconel625+20% Inconel718 has the yield strength of 672 MPa.

### 4.4 Experiment result analysis

Table 10 lists the results of the analysis of variance (ANOVA) test regarding UTS of 60% SS316L+20% Inconel625+20% Ti6Al4V and 60% SS316L+20% Inconel625+20% Inconel718. According to Table 10, 60% SS316L+20% Inconel625+20% Ti6Al4V has significance value of 0.747, and 60% SS316L+20% Inconel625+20% Inconel718 has significance value of 0.104. This result indicates that 60% SS316L+20% Inconel625+20% Ti6Al4V has the higher UTS.

Table 11 lists the results of ANOVA test regarding YS of 60% SS316L+20% Inconel625+20% Ti6Al4V and 60% SS316L+20% Inconel625+20% Inconel718. According to Table 11, 60% SS316L+20% Inconel625+20% Ti6Al4V has significance value of 0.829, and 60% SS316L+20% Inconel625+20% Inconel718 has significance value of 0.896. This result indicates that 60% SS316L+20% Inconel625+20% Ti6Al4V has the higher YS.

Table 12 lists the results of ANOVA test regarding elongation of 60% SS316L+20% Inconel625+20% Ti6Al4V and 60% SS316L+20% Inconel625+20% Inconel718. According to Table 12, 60% SS316L+20% Inconel625+20% Ti6Al4V has significance value of 0.996, and 60% SS316L+20% Inconel625+20% Inconel718 has significance value of 0.448. This result indicates that 60% SS316L+20% Inconel625+20% Ti6Al4V has the higher elongation.

**Table 10 ANOVA test results of UTS**

| Parameter | | Sum of squares | Degree of freedom | Mean square | *F* factor | Significance |
|---|---|---|---|---|---|---|
| 60% SS316L+20% Inconel625+20% Ti6Al4V | Between groups | 0.752 | 3 | 0.251 | 0.501 | 0.747 |
| | Within groups | 0.500 | 1 | 0.500 | - | - |
| | Total | 1.252 | 4 | - | - | - |
| 60% SS316L+20% Inconel625+20% Inconel718 | Between groups | 0.743 | 3 | 0.248 | 49.533 | 0.104 |
| | Within groups | 0.005 | 1 | 0.005 | - | - |
| | Total | 0.748 | 4 | - | - | - |

**Table 11 ANOVA test results of YS (0.2% proof)**

| Parameter | | Sum of squares | Degree of freedom | Mean square | *F* factor | Significance |
|---|---|---|---|---|---|---|
| 60% SS316L+20% Inconel625 +20% Ti6Al4V | Between groups | 0.672 | 3 | 0.224 | 0.311 | 0.829 |
| | Within groups | 0.720 | 1 | 0.720 | - | - |
| | Total | 1.392 | 4 | - | - | - |
| 60% SS316L+20% Inconel625 +20% Inconel718 | Between groups | 1.128 | 3 | 0.376 | 0.188 | 0.896 |
| | Within groups | 2.000 | 1 | 2.000 | - | - |
| | Total | 3.128 | 4 | - | - | - |

**Table 12 ANOVA test results of elongation**

| Parameter | | Sum of squares | Degree of freedom | Mean square | *F* factor | Significance |
|---|---|---|---|---|---|---|
| 60% SS316L+20% Inconel625 +20% Ti6Al4V | Between groups | 0.008 | 2 | 0.004 | 0.004 | 0.996 |
| | Within groups | 2.000 | 2 | 1.000 | - | - |
| | Total | 2.008 | 4 | - | - | - |
| 60% SS316L+20% Inconel625 +20% Inconel718 | Between groups | 0.623 | 2 | 0.312 | 1.234 | 0.448 |
| | Within groups | 0.505 | 2 | 0.253 | - | - |
| | Total | 1.128 | 4 | - | - | - |

**Table 13 ANOVA test results of hardness HRC**

| Parameter | | Sum of squares | Degree of freedom | Mean square | *F* factor | Significance |
|---|---|---|---|---|---|---|
| 60% SS316L+20% Inconel625 +20% Ti6Al4V | Between groups | 0.727 | 3 | 0.242 | 0.134 | 0.928 |
| | Within groups | 1.805 | 1 | 1.805 | - | - |
| | Total | 2.532 | 4 | - | - | - |
| 60% SS316L+20% Inconel625 +20% Inconel718 | Between groups | 0.343 | 3 | 0.114 | 0.282 | 0.844 |
| | Within groups | 0.405 | 1 | 0.405 | - | - |
| | Total | 0.748 | 4 | - | - | - |

Table 13 lists the results of ANOVA test regarding hardness HRC of 60% SS316L+20% Inconel625+20% Ti6Al4V and 60% SS316L+20% Inconel625+20% Inconel718. According to Table 13, 60% SS316L+20% Inconel625+20% Ti6Al4V has significance value of 0.928, and 60% SS316L+20% Inconel625+20% Inconel718 has significance value of 0.844. This result indicates that 60% SS316L+20% Inconel625+20% Ti6Al4V has the higher hardness.

Table 14 and Table 15 represent the ANOVA test regarding the elongation (represented by cross sectional area) of 60% SS316L+20% Inconel625+20% Ti6Al4V and 60% SS316L+20% Inconel625+20% Inconel718, respectively. According to Table 14, 60% SS316L+20% Inconel625+20% Ti6Al4V has significance value of 0.668; according to Table 15, 60% SS316L+20% Inconel625+20% Inconel718 has significance value of 0.693. This result indicates that 60% SS316L+20% Inconel625+20% Inconel718 has higher elongation.

Table 16 lists the results of ANOVA test regarding hardness (HB) of 60% SS316L+20% Inconel625+20% Ti6Al4V and 60% SS316L+20% Inconel625+20% Inconel718. According to Table 16, 60% SS316L+20% Inconel625+20% Ti6Al4V has significance value of 0.203, and 60% SS316L+20% Inconel625+20% Inconel718 has significance value of 0.907. This result indicates that 60% SS316L+20% Inconel625+20%

**Table 14 ANOVA test results of cross sectional area of 60% SS316L+20% Inconel625+20% Ti6Al4V**

| Parameter | Sum of squares | Degree of freedom | Mean square | *F* factor | Significance |
|---|---|---|---|---|---|
| Between groups | 0.402 | 2 | 0.201 | 0.496 | 0.668 |
| Within groups | 0.810 | 2 | 0.405 | - | - |
| Total | 1.212 | 4 | - | - | - |

**Table 15 ANOVA test results of cross sectional area of 60% SS316L+20% Inconel625+20% Inconel718**

| Parameter | Sum of squares | Degree of freedom | Mean square | *F* factor | Significance |
|---|---|---|---|---|---|
| Between Groups | 0.807 | 3 | 0.269 | 0.664 | 0.693 |
| Within Groups | 0.405 | 1 | 0.405 | - | - |
| Total | 1.212 | 4 | - | - | - |

**Table 16 ANOVA test results of hardness HB**

| Parameter | | Sum of squares | Degree of freedom | Mean square | *F* factor | Significance |
|---|---|---|---|---|---|---|
| 60% SS316L+20% Inconel625 +20% Ti6Al4V | Between groups | 4.763 | 3 | 1.588 | 12.701 | 0.203 |
| | Within groups | 0.125 | 1 | 0.125 | - | - |
| | Total | 4.888 | 4 | - | - | - |
| 60% SS316L+20% Inconel625 +20% Inconel718 | Between groups | 0.063 | 3 | 0.021 | 0.168 | 0.907 |
| | Within groups | 0.125 | 1 | 0.125 | - | - |
| | Total | 0.188 | 4 | - | - | - |

Inconel718 has the higher hardness.

### 4.5 Findings

From ANOVA analysis presented above, 60% SS316L+20% Inconel625+20% Inconel718 exhibits higher tensile strength than both the 60% SS316L+20% Inconel625+20% Ti6Al4V and the parent material SS316L. Similarly, the ANOVA analysis of YS indicates that the 60% SS316L+20% Inconel625+20% Inconel718 has the largest significant value, compared to the 60% SS316L+20% Inconel625+20% Ti6Al4V. However, 60% SS316L+20% Inconel625+20% Ti6Al4V shows higher elongation than 60% SS316L+20% Inconel625+20% Inconel718. Additionally, 60% SS316L+20% Inconel625+20% Inconel718 possesses the highest hardness among three experiment FGMs. Besides, 60% SS316L+20% Inconel625+20% Inconel718 has the largest cross-sectional area and the highest hardness (HB) compared to the 60% SS316L+20% Inconel625+20% Ti6Al4V and the parent material SS316L.

### 4.6 Discussion

From the analysis of the accumulated data, the testing was evaluated using statistic package for social science (SPSS), and conclusions are drawn as follows. The results indicate that FGM of 60% SS316L+20% Inconel625+20% Inconel718 has significantly greater strength, particularly due to the FGM of 60% SS316L+20% Inconel625+20% Ti6Al4V. The 60% SS316L+20% Inconel625+20% Ti6Al4V shows superior UITS and YS compared to SS316L.

## 5 Conclusions

A graded component that lacks a well-defined boundary composition was successfully fabricated using Inconel625 in conjunction with Ti6Al4V through WAAM. It is evident that numerous cracks occur during tensile testing of SS316L and Inconel625. For the specimens that were not preheated, cracks appear in the transition zones[9]. This study demonstrates that preheating treatment is an effective method for enhancing deposition and mitigating crack formation in Inconel625/Ti6Al4V FGMs. After experiencing multiple breakages and cracks, the manufactured FGM containing Ti6Al4V underwent comprehensive testing, yielding UTS of 686 MPa, hardness of 16 HRC, and elongation of 44%. These findings confirm that 60% SS316L+20% Inconel625+20% Ti6Al4V is a highly effective metal material. The test results further conclude that the 60% SS316L+20% Inconel625+20% Inconel718 is the optimal material for high-pressure pneumatic use and defence applications. The results of the mechanical property tests demonstrate that the 60% SS316L+20% Inconel625+20% Inconel718 exhibits the highest UTS and YS compared to both 60% SS316L+20% Inconel625+20% Ti6Al4V and the parent material SS316L. However, the 60% SS316L+20% Inconel625+20% Ti6Al4V shows superior UITS and YS compared to SS316L. Every study has its own limitations that can affect the accuracy of the results. This study also has certain limitations that may impact the attainment of accurate outcomes related to the research objectives. This study primarily focuses on the strength of the material, specifically examining YS, UTS, and hardness. Therefore, future research should further analyse other critical parameters, including vibration, impact, and corrosion behavior at high and low temperatures.

## References


1 Chen B, Su Y, Xie Z H *et al*. *Optics & Laser Technology*[J], 2020, 123: 105916

2 Jin W W, Zhang C Q, Jin S Y *et al*. *Applied Sciences*[J], 2020, 10(5): 1563

3 Yusuf S M, Cutler S, Gao N. *Metals*[J], 2019, 9(12): 1286

4 Segura-Cardenas E, Ramirez-Cedillo E, Sandoval-Robles J A *et al*. *Metals*[J], 2017, 7(12): 521

5 Barros R, Silva F J G, Gouveia R M *et al*. *Metals*[J], 2019, 9(12): 1290

6 Mukherjee T, DebRoy T. *Science and Technology of Welding and Joining*[J], 2019, 24(5): 412

7 Feenstra D R, Banerjee R, Fraser H L *et al*. *Current Opinion in Solid State and Materials Science*[J], 2021, 25(4): 100924

8 Tomar B, Shiva S, Nath T. *Materials Today Communications*[J], 2022, 31: 103739

9 Rodrigues T A, Farias F W C, Zhang K *et al*. *Journal of Materials Research and Technology*[J], 2022, 21: 237

10 Bhavar V, Kattire P, Thakare S *et al*. *IOP Conference Series: Materials Science and Engineering*[J], 2017, 229(1): 012021

11 Udupa G, Rao S S, Gangadharan K V. *Procedia Materials Science*[J], 2014. 5: 1291

12 Chen Y T, Liou F. *2018 International Solid Freeform Fabrication Symposium*[C]. Austin: University of Texas at Austin, 2018

13 Zhu J C, Lai Z H, Yin Z D *et al*. *Materials Chemistry and Physics*[J], 2001, 68(1–3): 130

14 Watanabe Y, Sato H. *Nanocomposites with Unique Properties and Applications in Medicine and Industry*[M]. London: IntechOpen, 2011: 150

15 Zhang B B, Jaiswal P, Rai R *et al*. *Journal of Computing and Information Science in Engineering*[J], 2018. 18(4): 041002

16 Kunimine T, Sato H, Miura-Fujiwara E *et al*. *Advances in Functionally Graded Materials and Structures*[M]. London: IntechOpen, 2016

17 Mahamood R M, Akinlabi E T, Shukla M *et al*. *Proceedings of the World Congress on Engineering 2012*[C]. London: International Association of Engineers, 2012

18 Yan L, Chen Y T, Liou F. *Additive Manufacturing*[J], 2020, 31: 100901

19 Efraim E. *Procedia Engineering*[J], 2011, 10: 242

20 Özdemir N, Bilgin B. *The International Journal of Advanced Manufacturing Technology*[J], 2009, 41: 519

21 Dey H C, Ashfaq M, Bhaduri A K *et al*. *Journal of Materials Processing Technology*[J], 2009, 209(18–19): 5862

22 Ghosh M, Chatterjee S. *Materials Characterization*[J], 2002, 48(5): 393
23 Lotfian S, Rolink G, Weisheit A *et al*. *MRS Advances*[J], 2017, 2(26): 1393
24 Carroll B E, Otis R A, Borgonia J P *et al*. *Acta Materialia*[J], 2016, 108: 46
25 Bobbio L D, Bocklund B, Simsek E *et al*. *Additive Manufacturing*[J], 2022, 51: 102649
26 Sahasrabudhe H, Harrison R, Carpenter C *et al*. *Additive Manufacturing*[J], 2015, 5: 1
27 Hosseini S R E, Feng K, Nie P L *et al*. *Optics & Laser Technology*[J], 2019, 112: 379
28 Li W, Karnati S, Kriewall C *et al*. *Additive Manufacturing*[J], 2017, 14: 95
29 Balla V K, De Vas Con Cellos P D, Xue W *et al*. *Acta Biomaterialia*[J], 2009, 5(5): 1831
30 Vishnukumar M, Muthupandi V, Jerome S. *Materials Letters*[J], 2022, 307: 131015
31 Kumar D S M, Yugeshkrishnan M, Santhoshkumar K *et al*. *The Scientific Temper*[J], 2023, 14(2): 405
32 Sasikumar R, Kannan A R, Kumar S M *et al*. *CIRP Journal of Manufacturing Science and Technology*[J], 2022, 38: 230
33 Li T X, Wang Z J, Hu S S *et al*. *Journal of Manufacturing Processes*[J], 2022, 82: 461
34 Meng W, Yin X H, Zhang W *et al*. *Journal of Materials Processing Technology*[J], 2020, 275: 116368
35 Rodrigues T A, Bairrão N, Farias F W C *et al*. *Materials & Design*[J], 2022, 213: 110270
36 Athaib N H, Haleem A H, Al-Zubaidy B. *Journal of Physics: Conference Series*[J], 2021, 1973(1): 012083
37 Sorger G L, Oliveira J P, Inácio P L *et al*. *Journal of Materials Science & Technology*[J], 2019, 35(3): 360
38 Wu W, Xue J X, Wang L L *et al*. *Metals*[J], 2019, 9(1): 109
39 Feng Y H, Zhan B, He J *et al*. *Journal of Materials Processing Technology*[J], 2018, 259: 206
40 Hosseini V, Högström M, Hurtig K *et al*. *Welding in the World*[J], 2019, 63: 975
41 Xiong J, Li Y J, Li R *et al*. *Journal of Materials Processing Technology*[J], 2018, 252: 128
42 Baufeld B, Biest O, Gault R. *International Journal of Materials Research*[J], 2009, 100(11): 1536
43 Herzog D, Seyda V, Wycisk E *et al*. *Acta Materialia*[J], 2016, 117: 371
44 Geng H B, Li J L, Xiong J T *et al*. *Journal of Materials Processing Technology*[J], 2017, 243: 40
45 Wang L L, Xue J X, Wang Q. *Materials Science and Engineering A*[J], 2019, 751: 183
46 Scotti A, Ponomarev V, Lucas W. *Journal of Materials Processing Technology*[J], 2014, 214(11): 2488
47 Hejripour F, Binesh F, Hebel M *et al*. *Journal of Materials Processing Technology*[J], 2019, 272: 58
48 Thompson S M, Bian L, Shamsaei N *et al*. *Additive Manufacturing*[J], 2015, 8: 36
49 Huang S W, Samandi M, Brandt M. *Wear*[J], 2004, 256(11–12): 1095
50 Walker K F, Lourenço J M, Sun S *et al*. *International Journal of Fatigue*[J], 2017, 94(2): 288
51 Li W, Zhang J W, Zhang X C *et al*. *Manufacturing Letters*[J], 2017, 13: 39
52 Ferreira A, Romio P, Sousa J *et al*. *Prime Archives in Material Science*[M]. Hyderabab: Vide Leaf, 2021

# 高压气动工具用SS316L/Inconel625基复合功能梯度材料的设计与开发

Sainath Krishna Mani Iyer[1]，Karuppasamy Ramasamy[1]，Prabagaran Subramaniam[2]
(1. 卡帕加姆高等学院 工程学院 机械工程系，印度 科钦巴托尔 641 021)
(2. 卡帕加姆创新与孵化委员会，印度 科钦巴托尔 641 021)

**摘　要：**通过电弧增材制造技术，将SS316L合金和Inconel625合金与Ti6Al4V或Inconel718合金结合，制备功能梯度材料（FGMs）。制备了2种FGMs，分别为60% SS316L+20% Inconel625+20% Ti6Al4V复合材料和60% SS316L+20% Inconel625+20% Inconel718复合材料。对抗拉伸强度、伸长率、屈服强度、硬度、母材的横截面积和成分进行了分析。结果表明，与60% SS316L+20% Inconel625+20% Ti6Al4V复合材料相比，60% SS316L+20% Inconel625+20% Inconel718复合材料具有更好的力学性能；同时，60% SS316L+20% Inconel625+20% Ti6Al4V复合材料的综合性能优于母材SS316L。因此，60% SS316L+20% Inconel625+20% Inconel718复合材料是最佳选择。由于其高强度，60% SS316L+20% Inconel625+20% Inconel718复合材料在高压气动工具和防御工具中具有巨大的应用潜力。

**关键词：**微观结构；抗拉伸强度；功能梯度材料；增材制造；Inconel合金；钛；不锈钢；电弧增材制造

作者简介：Sainath Krishna Mani Iyer，男，1987年生，硕士，工程师，卡帕加姆高等学院工程学院机械工程系，印度 科钦巴托尔 641 021，E-mail：sainath0318@gmail.com